International Journal of Concrete Structures and Materials
DOI 10.1186/s40069-018-0244-9
ISSN 1976-0485 / eISSN 2234-1315

Blast and Impact Analyses of RC Beams Considering Bond-Slip Effect and Loading History of Constituent Materials

MinJoo Lee and Hyo-Gyoung Kwak*

(Received February 1, 2017, Accepted January 15, 2018)

Abstract: An improved numerical model that can simulate the nonlinear behavior of reinforced concrete beams subjected to blast and impact loadings is introduced in this paper. The layered section approach is based in the formulation, and the dynamic material behaviors of concrete and steel are defined with the use of the dynamic increase factor. Unlike the classical layered section approach that usually gives conservative structural responses because of no consideration of the bond-slip effect, the introduced numerical model takes into account the bond-slip between reinforcing steel and surrounding concrete by changing the bending stiffness EI of elements placed within the plastic hinge length. Since the bond-slip developed after yielding of reinforcing steel is dominant and accompanies fixed-end rotation, the equivalent bending stiffness to be used in the critical region can be evaluated on the basis of the compatibility condition. In advance, the consideration of the unloading and reloading histories of reinforcing steel and concrete makes it possible to exactly trace the structural behavior even after reaching the maximum structural response. Finally, correlation studies between analytical results and experimental data are conducted to establish the validity of the introduced numerical model, and the obtained results show that it is important to consider the bond-slip effect and the loading history of constituent materials.

Keywords: blast, impact, layered section approach, high strain rate, bond-slip, loading history of constituent material.

1. Introduction

Due to an increase of accidental explosions and terrorist acts of bombing worldwide, a lot of researches to reserve the safety of structures under blast and impact loadings, which were originally limited to military facilities, have been conducted with considerable attention to civil structures (Kwak and Gang 2015; Lin et al. 2014; Luccioni et al. 2004). Since explosions usually cause severe damage to structures with loss of human lives, blast protection of structures is strongly required and can be achieved through accurate prediction of structural responses. In particular, recent increases in the size and height of structures have accelerated the need to secure structural resistance to blast and impact loadings.

Reinforced concrete (RC) structures subjected to blast and impact loadings exhibit remarkably different structural behavior from that observed under a quasi-static loading condition due to the change in the material properties of concrete and reinforcing steel at a high strain rate condition (Carta and Stochino 2013; Qu et al. 2016; Valipour et al. 2009). Thus, the accurate prediction of structural behaviors in RC structures subjected to blast or impact loadings will be possible through an exact implementation of the high strain rate deformations in concrete and reinforcing steel that occur during a short period of time and the nonlinearity such as the bond-slip effect that dominantly affects the resisting capacity of RC structures. Furthermore, consideration of the loading history of constituent materials, which is expressed through the description of loading, unloading, and reloading, is also required to precisely trace the structural response even after the application of blast and impact loadings.

In this context, many studies, from experiments to identify the strain rate dependent material properties (Cadoni et al. 2009; Cusatis 2011) to numerical analyses of RC structures under impact loading (Fujikake et al. 2009; Tachibana et al. 2010), have been conducted. Nevertheless, it is also true that few experimental results for RC structural members subjected to blast and impact loadings can be found in the literature due not only to national security reasons but also to the fact that experiments are costly, time consuming and difficult to carry out. To overcome these difficulties in dynamic experiments, numerous analytical approaches from a simple approach such as a single degree of freedom model (Biggs 1964) to a rigorous finite element analysis using numerous solid elements (Chen et al. 2012; Jones et al. 2009; Ožbolt and Sharma 2011) have been proposed to verify the structural responses of RC structures. The obtained research results have been used in developing design codes such as the CEB-FIP model code (Comite Euro-International 1993) and ACI 318-08 (ACI Committee

Department of Civil and Environmental Engineering, KAIST, Daejeon 34141, Republic of Korea.
*Corresponding Author; E-mail: kwakhg@kaist.ac.kr

Published online: 27 March 2018

and ACI 2008), and also have been implemented into many commercialized programs including LS-DYNA (LSTC 2007) and ABAQUS (Hibbitt and Karlsson and Sorenson Inc. 2001) to be used in tracing the nonlinear response of RC structures subjected to blast and impact loadings.

Nevertheless, most numerical methods still accompany some problems when applied to RC beams. The use of solid elements gives mesh-dependent numerical results (Kwak and Gang 2015) and necessitates choosing one of the three dimensional failure criteria for concrete even though these criteria cannot simulate the concrete cracking behavior accurately (Tu and Lu 2009; Wu et al. 2012). A single degree of freedom (SDOF) model also has some limitations in simulating the nonlinear response of RC beams, even though it has been popularly adopted in design practice because of ease-of-use. Since the SDOF method not only adopts a lot of approximations but also cannot exactly take into account the nonlinear behavior in a RC section induced from the cracking of concrete and yielding of reinforcing steel, the use of the SDOF method may be inappropriate when a precise evaluation of the structural response is required.

The use of beam elements is also not exceptional. The beam model cannot consider the bond-slip effect between reinforcing steel and surrounding concrete because the strain compatibility has been based upon the perfect bond assumption (Bicanic et al. 2011). This restriction makes it more difficult to take into account the fixed-end rotation which occurs after yielding of the main reinforcement. The nonlinear analyses of RC beams consequently may give different results by ignoring the bond-slip effect, and in advance, the accuracy of the simulation results may not be guaranteed. Nevertheless, the bond-slip effect is still excluded in the numerical formulation of RC beams subjected to blast and impact loadings (Yao et al. 2016).

To address these limitations in the numerical analyses of RC beams, this paper presents a numerical model developed to consider the bond-slip effect in a beam element. The layered section method is based in the formulation, and the dynamic material behaviors of concrete and steel are defined with the use of the dynamic increase factor (DIF). The very different feature of the introduced numerical model is the implementation of the bond-slip effect, which cannot be considered in the classical layered section approach because of the difficulty in defining the relative slip along the reinforcing steel. In order to take into account the influence of bond-slip, the proposed numerical model suggests using the equivalent bending stiffness EI_{eq} within the plastic hinge length, upon the assumption that a large portion of the bond-slip will be concentrated, due to the anchorage slip, within the plastic hinge length where the yielding of reinforcing steel is subjected. Based on the compatibility condition, the equivalent bending stiffness EI_{eq} to be used in the critical region is evaluated.

In advance, the consideration of the loading histories of reinforcing steel and concrete makes it possible to exactly trace the structural behavior even after reaching the maximum structural response. Since the residual structural response beyond the maximum structural response is due to the unloading and reloading behavior of constituent materials, its exactness will be directly related to the consideration of the loading history for reinforcing steel and concrete. Finally, the validity of the proposed numerical model is confirmed by the comparison of analytical predictions with experimental data. Furthermore, the effects of bond-slip and loading history of the constituent materials are discussed through parametric studies, and the obtained results show the importance of considering both effects in the nonlinear dynamic behavior of RC beams subjected to blast and impact loadings.

2. Material Properties

2.1 Concrete

Since the equilibrium equation of a RC beam element, which is divided into imaginary layers to represent the different material properties, is constructed on the basis of the constitutive relationships in a layer, the behavior of RC beams subjected to external loads is highly dependent on the used material model and the magnitude of stress. Among the various available mathematical models currently used in the numerical analyses of RC structures, the monotonic envelope curve proposed by Kent and Park (1971) and later extended by Scott et al. (1982) is adopted in this paper because of its simplicity and computational efficiency (see Fig. 1a). More details of the stress–strain relation to define the envelope curve can be found elsewhere (Kwak and Hwang 2010).

For the tensile region, concrete is linearly elastic up to the tensile strength. Beyond that, the tensile stress decreases along a linear softening branch with increasing principal tensile strain. It is assumed that ultimate failure takes places by cracking, when the strain exceeds the value of ε_{t0} where b is the length of elements and G_f denotes the fracture toughness of concrete, as shown in Fig. 1b (Kwak and Hwang 2010).

After defining the monotonic envelope curve, it is necessary to exactly define the unloading–reloading behavior in order to describe the hysteretic response of concrete. However, the monotonic envelope curves are obtained on the basis of experimental studies, whereas the definition of an accurate cyclic stress–strain relation is very limited since it is difficult to carry out experiments for concrete subjected to cyclic loadings. Only a few of cyclic constitutive models have been proposed through experimental results (Konstantinidis et al. 2007).

Since the exact definition of the unloading–reloading paths in cracked concrete is complex, while these nonlinear paths have a minor effect in describing the hysteretic behavior of RC structures, simplified relations are usually adopted to define the cyclic stress–strain relation of concrete. This paper also adopts a straight unloading–reloading relation to be used in the compression region [see Eq. (1)], as proposed by Karsan and Jirsa (1969) and later extended by Taucer et al. (1991) to remove unreasonable behavior under high

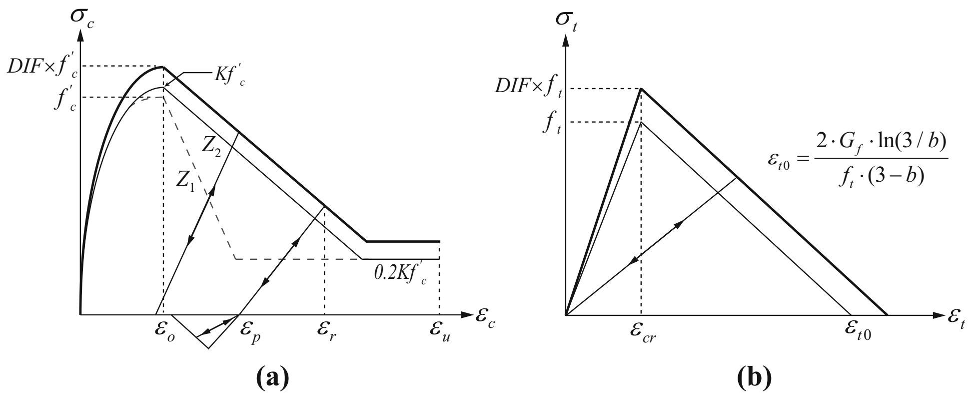

Fig. 1 Stress–strain relation of concrete. **a** Compression region and **b** tensile region.

compressive strain conditions, because it has been popularly used in the dynamic analyses of RC structures (Mashaly et al. 2011; Valipour et al. 2009).

$$\begin{aligned} \frac{\varepsilon_p}{\varepsilon_o} &= 0.145\times\left(\frac{\varepsilon_r}{\varepsilon_o}\right)^2+0.127\times\left(\frac{\varepsilon_r}{\varepsilon_o}\right), && \left(\frac{\varepsilon_r}{\varepsilon_o}\right)<2 \\ \frac{\varepsilon_p}{\varepsilon_o} &= 0.707\times\left(\frac{\varepsilon_r}{\varepsilon_o}-2\right)+0.834, && \left(\frac{\varepsilon_r}{\varepsilon_o}\right)\geq 2 \end{aligned} \tag{1}$$

where ε_r is the strain at which unloading starts to a point ε_p on the strain axis and ε_o is the strain corresponding to the maximum stress in compression. On the other hand, the unloading–reloading paths in the tension region are assumed to always pass the origin regardless of the loading history because their application is limited to RC beams in which the bending behavior is dominant. However, it is also true that the used unloading–reloading path does not account for the cyclic damage of concrete, but the importance of this effect on the hysteretic behavior of RC beams is beyond the scope of this paper.

It is shown that the dynamic compressive and tensile strengths of concrete under rapid loading increase significantly due to the lateral inertia confinement effect and the change of the crack pattern (Yan and Lin 2006). Previous experimental studies provide a more detailed description of strain rate effects on concrete (Cusatis 2011). Moreover, many mathematical models have also been proposed, which express an increase in strength and critical strain depending on the strain rate (Hao et al. 2012; Shkolnik 2008). In spite of many accurate numerical models for the consideration of the strain rate effect, however, the simple relations introduced by Saatcioglu et al. (2011) are adopted in this paper for computational convenience.

This model introduced a dynamic increase factor (DIF) to take into account the strain rate effect, and the compressive and tensile strength under a high strain rate condition can be determined by multiplying the DIF corresponding to the developed strain rate. Nevertheless, the strain at peak stress and the shape of the descending branch were assumed to be constant regardless of the change in the strain rate (see Fig. 1). This model requires only the strain rate $\dot{\varepsilon}$ to compute the dynamic strength increase in concrete and can be expressed as follows (Saatcioglu et al. 2011): $DIF=0.03\ln\dot{\varepsilon}+1.30\geq 1.0$ for $\dot{\varepsilon}<30\ \mathrm{s}^{-1}$, and $DIF=0.55\ln\dot{\varepsilon}-0.47$ for $\dot{\varepsilon}\geq 30\ \mathrm{s}^{-1}$. The same equations are used in compression and tension for the computational convenience because DIF values for compression and tension do not show a large difference in a structure subjected to general blast loading which accompanies the relatively small strain rate.

2.2 Steel

A bilinear stress–stain relation with the yield strength f_y, which assumes a linear elastic and linear strain hardening behavior, is usually used for reinforcing steel. On the other hand, the yield stress of the reinforcing bar surrounded by concrete needs to be reduced to f_n, as shown in Fig. 2. When the steel stress at the cracked section reaches the yield strength of the bare bar, the average steel stress at a cracked element still will be less than the yield strength, because of the tension stiffening effect in concrete. The concrete matrix located between cracks is still partially capable of resisting tensile forces, owing to the bond between the concrete and reinforcement. Thus, in the analysis of RC beams under cyclic loading which accompanies relatively large deformation, the use of the average stress–strain relation is

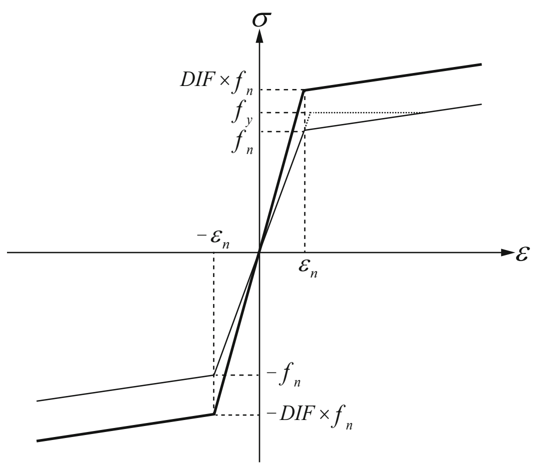

Fig. 2 Monotonic stress–strain relation of steel.

required (Belarbi and Hsu 1994), and this paper adopts the linearized average stress–strain relation proposed by Belarbi and Hsu (1994) as the revised monotonic envelope curve of steel.

$$\sigma_s = E_s \times \varepsilon_s, \qquad \varepsilon_s < \varepsilon_n$$
$$\sigma_s = f_y\left[(0.91 - 2A) + \left(0.02 + 0.25A\frac{\varepsilon_s}{\varepsilon_y}\right)\right], \qquad \varepsilon_s \geq \varepsilon_n \tag{2}$$

where ε_y and f_y denote the yield strain and stress of a bare steel bar, and ε_s and σ_s are the average strain and stress, respectively. The average stress σ_s is a linear function of the parameter $A = (f_t/f_y)^{1.5}/\rho$ and is limited by the boundary strain $\varepsilon_n = \varepsilon_y(0.93 - 2A)$ for the yielding of steel, where ρ represents the percentage of the steel ratio and must be greater than 0.5%. More details of the average stress–strain relation of steel can be found elsewhere (Belarbi and Hsu 1994).

The strain rate effect is considered by introducing a DIF (see Fig. 2), as mentioned in connection to Fig. 1. The relation of DIF as used by Saatcioglu et al. (2011) is adopted under the same assumption to define the dynamic stress–strain relation of reinforcing steel, and the corresponding equation is presented as follows: $DIF = 0.034\ln\dot{\varepsilon} + 1.30 \geq 1.0$.

Upon the definition of the monotonic envelope for reinforcing steel, the nonlinear model of Menegotto and Pinto (1973), which was modified by Filippou et al. (1983) to include isotropic strain hardening, was selected to define the unloading and reloading behavior because of its advantages such as easy estimation of parameters through comparison with experimental data and good representation of the Bauschinger effect. The unloading–reloading path can be defined as follows:

$$\sigma^* = b\varepsilon^* + \frac{(1-b)\varepsilon^*}{(1+\varepsilon^{*R})^{1/R}} \tag{3}$$

where $\sigma^* = (\sigma - \sigma_r)/(\sigma_o - \sigma_r)$, $\varepsilon^* = (\varepsilon - \varepsilon_r)/(\varepsilon_o - \varepsilon_r)$, σ_o and ε_o are the stress and strain at the point where the two asymptotes of the branch under consideration meet (see point A in Fig. 3); similarly, σ_r and ε_r are the stress and strain at the point where the last strain reversal with stress of equal sign took place (see point B in Fig. 3); b is the strain-hardening ratio between slope E_{S1} and E_{S2}, and R is a parameter that influences the shape of the transition curve and represents the Bauschinger effect. More details related to this model can be found elsewhere (Kwak and Kim 2006).

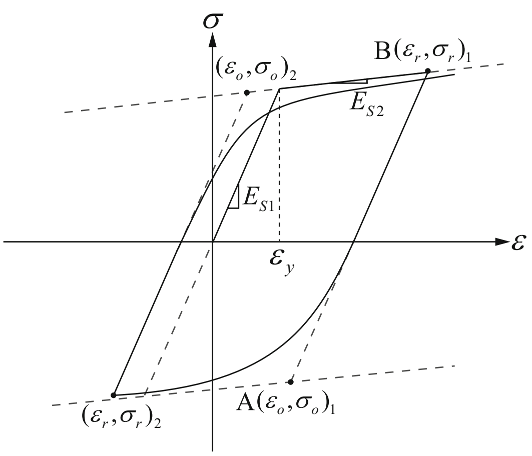

Fig. 3 Cyclic stress–strain relation of steel.

3. Consideration of Bond-Slip Effect

The perfect bond assumption usually adopted in the analysis of RC beams is reasonable only in uncracked regions where bond stress transferred along the interface between reinforcing steel and surrounding concrete is negligibly small (Monti and Spacone 2000). The influence of bond-slip, however, is particularly noticeable in a cracked region, and the bond-slip will be remarkably enlarged with the yielding of reinforcing steel (Kwak and Kim 2010). Therefore, consideration of the bond-slip effect is required to simulate the structural behavior more exactly.

In this regard, many studies have been conducted to consider this effect (Oliveira et al. 2008; Santos and Henriques 2015), and the bond-slip models such as the bond-link element and the bond-zone element have been introduced to take into account the bond-slip effect (Lowes et al. 2004). In these models, the relative slip between concrete and reinforcement is evaluated by using a double node. However, in a beam element defined by both end nodes along the length direction, it is impossible to use the double node at each end node. To address this limitation in adopting the bond model, a numerical algorithm that includes the bond-slip effect is proposed in this paper.

Since the critical region where the bending moment is larger than the yielding moment is usually located in the vicinity of the beam mid-span or both clamped ends of the beam, the bond-slip may be concentrated in this region. In particular, cracking in this critical region accompanies fixed-end rotation θ_{fe} in a RC beam, which has been induced from slippage of the main reinforcing steel (δ in Fig. 4) and cannot be simulated by any mechanical model (see Fig. 4). In advance, this rigid body deformation may increase with an increase of the deformation, which is about 50% of the total deformation. Accordingly, the fixed-end rotation, which

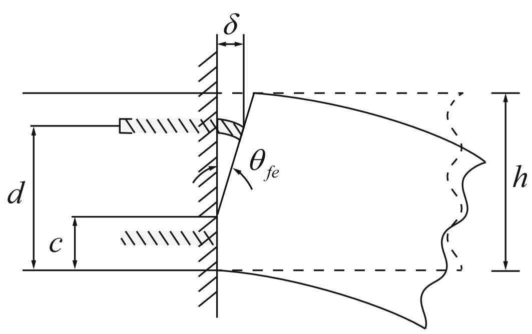

Fig. 4 Fixed-end rotation at the beam-column joint.

is induced by the slippage of the main reinforcement at the critical region, needs to be considered.

A half of a simply support RC beam can be considered as a free body diagram, as shown in Fig. 5a, because the critical region will be placed at the mid-span, where L_p is the plastic hinge length where the plastic deformation is concentrated and EI_{eq} represents the reduced bending stiffness caused by the concentrated bond-slip. For plastic hinge length, the relatively simple equation of $L_p = xh$ proposed by Bayrak and Sheikkh (1997) is used, where x is an experimentally determined parameter ranging from 0.9 to 1.0 and h is the section depth. As shown in Fig. 5a, if a point load P is applied at the mid-span of an RC beam, the maximum deflection $\Delta_1 = P \times (EI_{eq}L_1^3 + EIL_p(3L_pL_1 + 3L_1^2))/(3EI_{eq}EI)$ can be obtained by the moment area method.

In addition, the beam can also be idealized by using the equivalent rotational stiffness K_θ, as shown in Fig. 5b, because additional rigid body rotation, which causes a reduction of the bending stiffness, will be accompanied by slippage of the main reinforcement and can be simulated by introducing the end rotational stiffness. In this case, K_θ can be obtained by the ratio of the moment to the fixed-end rotation ($K_\theta = M_y/\theta_{fe}$) and, the fixed-end rotation is determined by the relation of $\theta_{fe} = \delta/(d - c)$, where δ denotes the bond-slip of the reinforcing steel (see Fig. 4), and d and c are the effective depth in an RC section and the distance from the extreme compression fiber to the neutral axis, respectively.

If the same load P acts on the beam with the rotational stiffness K_θ at the mid-span, the mid-span deflection of the beam Δ_2 can be evaluated in Fig. 5b as $\Delta_2 = PL^3/3EI + PL^2/2K_\theta$, where the first term accounts for the deformation due to bending and the second represents the contribution by the rigid body rotation. Then, from the equality between Δ_1 and Δ_2, the equivalent bending stiffness EI_{eq} can be determined as the following relation.

$$\frac{1}{EI_{eq}} = \frac{1}{\beta \times K_\theta \times L} + \frac{1}{EI} \tag{4}$$

where $\beta = \alpha(1 - \alpha + 1/3\alpha^2)$ and $\alpha = L_p/L$. The proportional constant β is dependent on the boundary condition, and the obtained expression for the proportional constant can be applied to a simply supported or cantilevered beam. The same derivation procedure can also be applied to RC beams with other boundary conditions, and the same expression as in Eq. (4) is obtained. The only difference is the value of β, which has the expression of $\beta = \alpha(1 - 2\alpha + 4/3\alpha^2)$ for a both clamped boundary condition. In advance, even with different loading type such as a uniformly distributed load by blast loading, the same derivation procedure can be applied, and the obtained expression for the constant β in a simply supported beam has the expression of $\beta = \alpha(1 - 1/2\alpha - 1/3\alpha^2 + 1/4\alpha^3)$.

Since the bond-slip δ can be evaluated on the basis of the assumption that the crack width ω caused by the bending behavior is equivalent to two times the bond-slip ($0.5\omega = \delta$) at the considered position, and the crack width can directly be evaluated by the formula introduced by Gergely and Lutz (1968), the rotational stiffness K_θ can be evaluated from $K_\theta = M_y/\theta_{fe} = M_y(d - c)/\delta$. Moreover, Eq. (4) not only gives the equivalent bending stiffness EI_{eq} but also takes into account the strain rate dependent bond-slip effect indirectly, and the modification of the bending stiffness of the elements within the plastic hinge length will be followed.

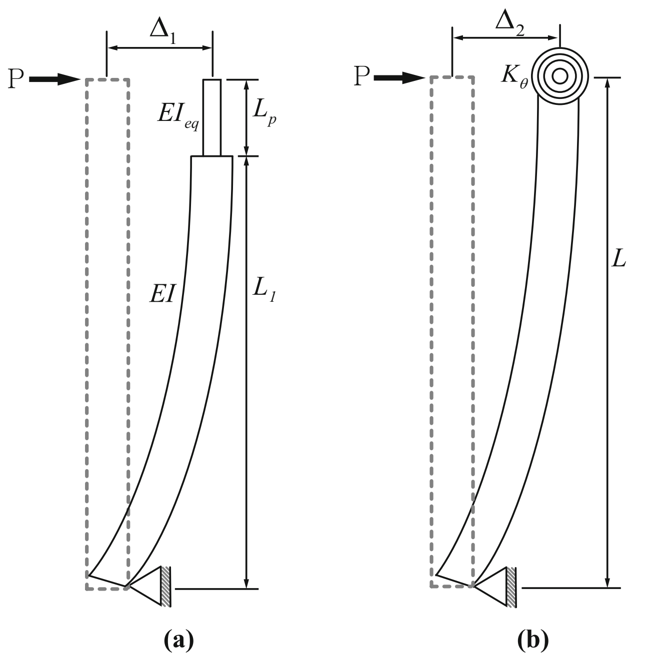

Fig. 5 Half-span RC column considering the equivalent bending stiffness EI_{eq}. **a** Simplified model with EI_{eq} and **b** equivalent model with K_θ.

4. Solution Procedure

To analyze RC beams subjected to blast and impact loadings, the construction of an element stiffness is based on the layered Timoshenko beam theory, which takes the shear deformation into consideration, and this paper adopts the Newmark method, in which a constant average acceleration with Newmark coefficients of $\beta = 0.25$ and $\gamma = 0.5$ is based. More details related to the construction of the element stiffness and the numerical evaluation of the dynamic response can be found elsewhere (Ayoub and Filippou 1999).

In advance, to minimize the difference in numerical results according to the finite element mesh size, as was mentioned in a previous study (Kwak and Gang 2015), all the RC beams considered in this paper have been idealized by ten elements through a convergence test. On the other hand, the critical regions within the plastic hinge length are discretized by the use of two elements to accurately estimate the plastic deformation especially after yielding of reinforcing steel because such a separate consideration of the critical region is required to avoid overestimation of the ultimate resisting capacity and underestimation of the developed lateral deformation.

5. Numerical Applications

In order to establish the validity and applicability of the proposed model, correlation studies between analytical results and experimental data are conducted using displacement–time curve, in which the mid-span displacements in specimens were measured by potentiometers attached at mid-span. Among the numerous experimental results that are available in the literature, seven simply supported RC beams are investigated and discussed, because these specimens represent typical structural behaviors according to various effects such as the steel ratio and loading type. The first two beams of B40_D1 and B40_D2 experimentally evaluated by Magnusson and Hallgren (2000) are considered to show the influence of the bond-slip effect on the structural behavior, and the next three beams of WE2, WE5 and WE6 experimented on by Seabold (1967) are considered to show the importance for considering the loading history of constituent materials in the post-peak response of RC beams. The last two specimens of SS3a and SS3b experimented on by Saatci (2007) are considered to verify the exactness of the introduced nonlinear dynamic algorithm. Especially, four specimens of B40_D2 to WE6 in Table 1 led to the shear failure in the experiments. However, since the main reinforcements of these specimens were yielded when the specimens developed the maximum displacements at mid-span, the bond-slip effect and the loading history of constituent materials are expected to deliver considerable influence on the structural behavior.

The material properties of each specimen are summarized in Table 1, and more details of the experimental setup can be found elsewhere (Magnusson and Hallgren 2000; Saatci 2007; Seabold 1967). Moreover, three beams B40_D1, B40_D2, and SS3a, among these specimens are also analyzed by using the equivalent SDOF model on the basis of the approach introduced at UFC-3-340-02 (US DoD 2008), to compare the accuracy of the proposed numerical model. To define the dynamic material properties of constituent materials in the SDOF, differently from the introduced numerical model, which considers the change of DIF according to the strain rate, a constant value of DIF = 1.2, which is corresponding to the minimum value among the mainly used DIF values ranged from 1.2 to 1.4 (Magnusson 2007; Fujikura and Bruneau 2011), is used, because the test specimens considered in this paper are subjected to relatively small blast loadings. To trace the post-peak nonlinear behavior of RC beams after the maximum loading history, the damping coefficient c is assumed to be about 3% of the critical damping ($C = 0.03C_{cr}$) because the experiments considered in this paper did not give any damping value. This value is usually considered in the nonlinear dynamic analyses of RC structures.

The SDOF analyses conducted in this paper are based on the transformation factors of mass (K_M), load (K_L) and stiffness (K_R), where the value of each factor is determined according to the boundary conditions, strain ranges (either elastic or plastic) and loading types. In this paper, average values of $K_M = 0.41$ and $K_L = K_R = 0.57$ were used because the structural response may be extended to the inelastic behavior. This modification was made according to Magnusson's suggestion (Magnusson 2007). The finally determined parameters for the SDOF model conducted by the standard procedure introduced at UFC-3-340-02 (US DoD 2008) are summarized in Table 2. The average acceleration method was used to evaluate the dynamic response of RC structures, and more details of the transformation of the multi-degree of freedom system into an equivalent SDOF system as well as the description of the average acceleration method can be found elsewhere (Biggs 1964; Craig Jr and Kurdila 2006; US DoD 2008).

The first two specimens are RC beams B40_D1 and B40_D2, and the geometric configuration and the description for the blast loading are represented in Fig. 6. The test setup is shown in Fig. 6a, and since the beams are placed within the shock tube at a distance of 10 m from explosive charge, the beams may be assumed to be exposed to a planer blast wave. As the blast wave strokes the closed end of the shock tube with the assembled beam, the wave reflects and a uniformly distributed load spreads across the surface of the beam (Magnusson 2007). The only difference between both specimens is the magnitude of the blast loading applied to the structure, and information for the applied blast loadings used in the experiments can be found in Table 3. Actual blast loading obtained from the experiment is idealized as simple triangular loading (see Fig. 6b). More details related to the experimental setup can also be found elsewhere (Magnusson and Hallgren 2000). In advance, to take into account the plastic hinge length in the finite element idealization, the specimens were modeled with an element length

Table 1 Material properties of each specimen.

Specimens	f_c (MPa)	f_y (MPa)	E_c (GPa)	E_s (GPa)	Reinforcement
B40_D1	43	595	31	205	5 ϕ 16 mm
B40_D2	43	595	31	205	5 ϕ 16 mm
WE2	27	457	27.3	199.8	2 No. 7/2 No. 9
WE5	27	462	27.3	199.8	2 No. 7/2 No. 9
WE6	28.4	455	27.3	199.8	2 No. 7/2 No. 9
SS3a	46.7	464	33	195	2 No. 30/2 No. 30
SS3b	46.7	464	33	195	2 No. 30/2 No. 30

Table 2 Parameter values for equivalent SDOF models.

Specimens	P_l (kN)	t_d (ms)	R_m (kN)	M (kg)	K (MN/m)
B40_D1	175	12	259	80	29
B40_D2	256	8.3	259	80	29.5
SS3a	1410	1.1[a]	428	668	31

P_l peak load, t_d time duration, R_m maximum resistance, M mass, K stiffness.
[a]Time up to peak impact load.

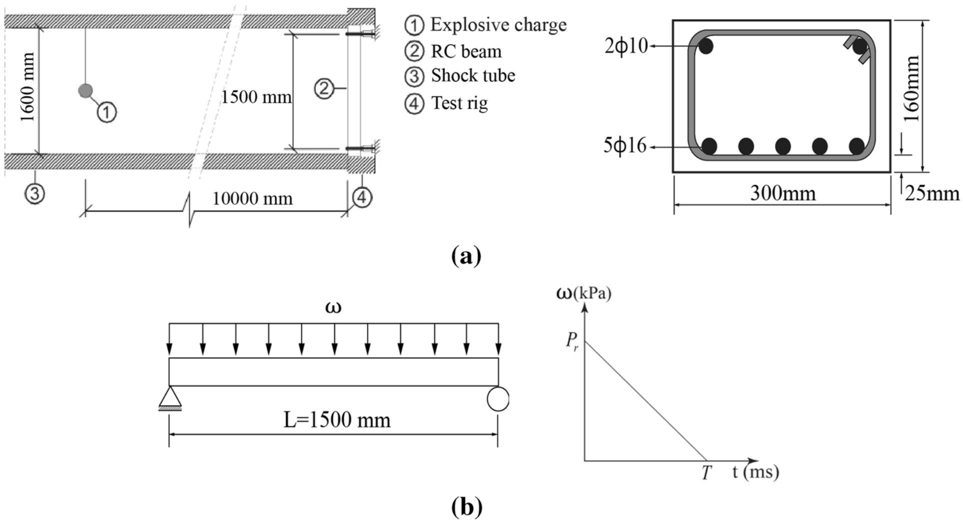

Fig. 6 Geometry and loading history for B40_D1 and B40_D2 (Magnusson and Hallgren 2000). **a** Experimental setup and section details and **b** configuration of B40_D1 and B40_D2 and blast loading.

Table 3 The details of blast loadings.

Specimens	Q (kg)	P_r (kPa)	T (s)
B40_D1	1.1	650 ± 31	0.023
B40_D2	2.0	1060 ± 116	0.026

Q mass of explosive charge, P_r maximum reflected pressure, T duration of the positive phase of the pressure–time history.

of $l = 140$ mm for the two elements at the mid-span, which is smaller than the calculated plastic hinge length of $l_p = 0.9 \times 160$ mm $= 144$ mm, and with an element length of $l = 152.5$ mm for the other eight elements.

Figures 7 and 8 present a comparison of the experimental results with the predicted results for the mid-span deflections with time for two specimens B40_D1 and B40_D2, respectively. As shown in these figures, a relatively close agreement between analyses and experiments was obtained in predicting the maximum displacement, and the evaluated displacement histories up to the maximum displacement are also almost coincident with those obtained from the experiments. This means that the introduced numerical model can effectively be used in the numerical analyses of RC beams subjected to blast loadings. These figures also show the significant difference between the numerical results depending on whether the bond-slip effect is considered, and this difference is gradually enlarged with an increase of the maximum displacement due to the yielding of reinforcing steel.

Moreover, the displacement time history for both specimens is also obtained by the SODF analysis. As shown in Figs. 7b and 8b, the SDOF model also shows a similar displacement history to the experimental data in the case of B40_D1 but a large difference from the experimental data in the case of B40_D2. This appears to be induced by the classical SDOF model not taking into account the bond-slip effect, which suddenly increased with the yielding of reinforcing steel. Accordingly, if the bond-slip effect can be implemented in the equivalent stiffness of the SDOF model, additional improvement in the numerical results can be expected.

On the other hand, since the blast loading for the beam B40_D1 is not large enough to develop yielding of tensile reinforcements, the results with and without consideration of the loading history of the constituent materials are almost the same even at the unloading stage (see Fig. 7a). A slight difference in numerical results according to the consideration of the loading history of materials can be found in beam B40_D2, which accompanies the yielding of tensile

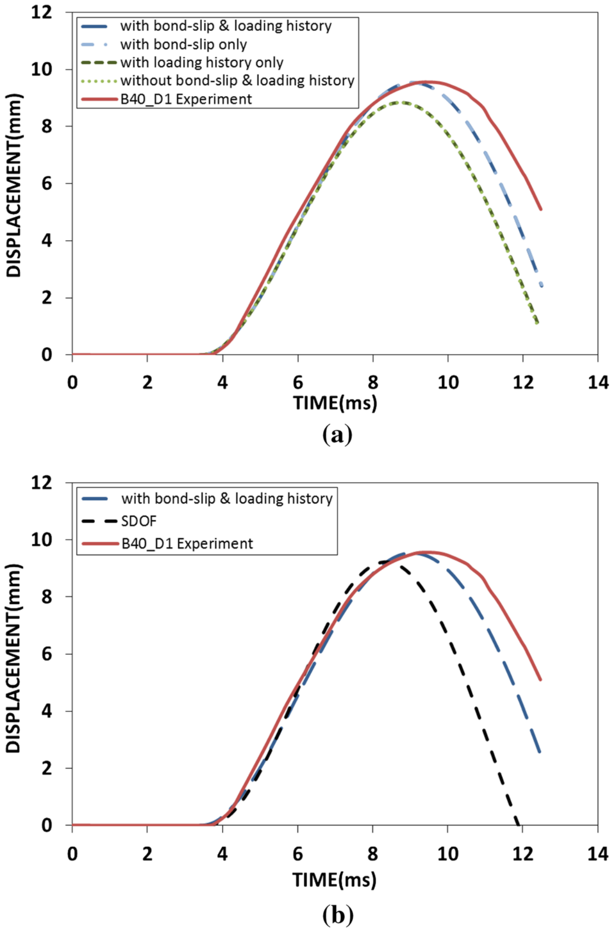

Fig. 7 Mid-span deflection with time for B40_D1. **a** Comparison with experiment and **b** comparison with SDOF model.

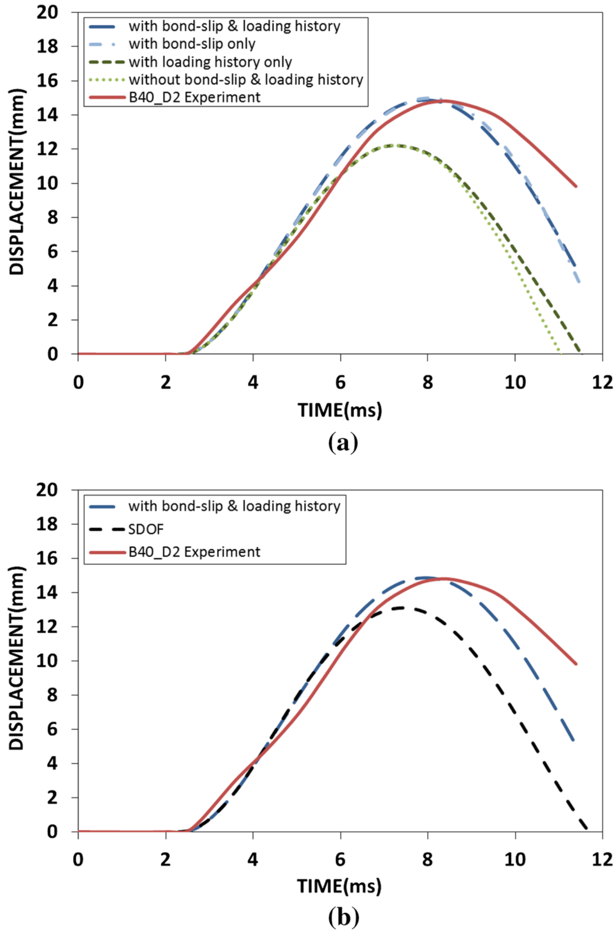

Fig. 8 Mid-span deflection with time for B40_D2. **a** Comparison with experiment and **b** comparison with SDOF model.

reinforcements (see Fig. 8). However, comparison of the displacement history limited to the first unloading behavior appears to be insufficient to exactly evaluate the influence of considering the loading history of the constituent materials.

To supplement this limitation, the next three RC beams of WE2, WE5, and WE6 subjected to the same uniformly distributed blast loading were considered, and the geometric configuration and the description for the blast loading are represented in Fig. 9. As shown in Fig. 9a, the specimens were tested by using the NCEL blast simulator, and a uniformly distributed dynamic load was delivered on the top surface of specimen through expansion of gases in the simulator (Seabold 1967). As shown in Fig. 9 and Table 1, the only differences in each specimen are the slight change in the compressive strength of concrete and the yield strength of reinforcing steel, and the applied blast loading was sufficient to cause the yielding of tensile reinforcements placed in these beams. These specimens were modeled with ten elements including two smaller elements at the mid-span whose length is $l = 341$ mm, which is less than the plastic hinge length of $l_p = 343$ mm.

Figure 10 shows the obtained displacement histories with time at the mid-span of the beams. In order to investigate the influence of the loading history in the constituent materials on the structural behavior, the numerical analyses were continued for longer time duration than that measured at the experiments. From the obtained results in Fig. 10, it is observed that the proposed model, in which both the bond-slip effect and the loading history of the constituent materials are considered, can reasonably predict the initial stiffness and the maximum displacement. In advance, the consideration of the loading history in steel and concrete does not affect the displacement history with time up to reaching the maximum displacement point because the constituent materials will be on the loading phase. However, after the maximum displacement point, the post-peak response is dominantly affected by the loading history of steel and concrete. In particular, since a large deformation of RC beams is induced from the ductile behavior of reinforcing steel after yielding, an exact prediction of the post-peak displacement history may depend on the exactness in defining the unloading and reloading behavior of reinforcing steel.

Moreover, the displacement history in Fig. 10 also shows that ignoring the loading history of the constituent materials lengthens the returning period in the displacement cycle. Since ignoring the loading history of materials leads the constituent materials to behavior along the loading path even at the unloading stage after developing large deformation, the stiffness of the structure will be underestimated compared to the real stiffness. This underestimation of the stiffness causes an increase of the returning period because

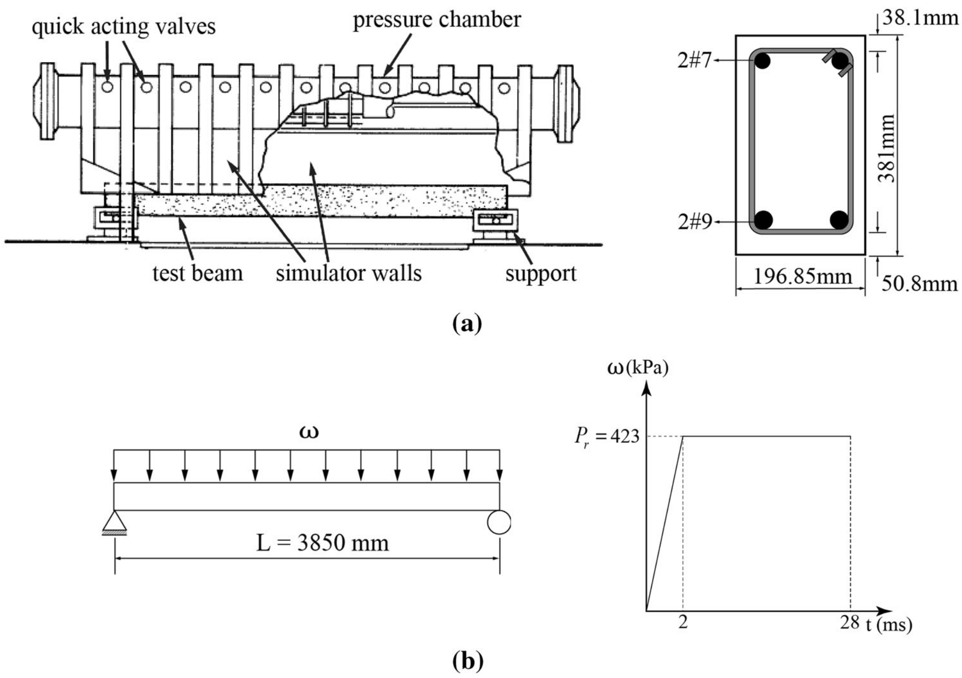

Fig. 9 Geometry and loading history for WE2, WE5, and WE6 (Seabold 1967). **a** Experimental setup and section details and **b** configuration of WE2, WE5, and WE6 and blast loading.

the period is inversely proportional to the stiffness of the structure. This result is induced by the fact that concrete and reinforcing steel under the unloading path represent larger stiffness, which is not substantially different from the initial stiffness. These differences in following the unloading path cause a large difference in the displacement history at the post-peak structural response, as shown in Fig. 10.

The last two specimens are the same RC beams of SS3a and SS3b subjected to different concentrated impact loadings through a dropping mass, and the geometric configuration and the description for the impact loading are given in Figs. 11 and 12, respectively. Beams SS3a and SS3b are subjected to a drop weight of 211 kg and a heavier one of 600 kg at the mid-span, respectively, and Fig. 12 shows the impact loading history measured in experiment. Since the introduced numerical model is based on the beam element which cannot take into account the contact behavior induced by the interaction of the dropping mass and the structure, the initial influence of the dropping mass on the structure is indirectly implemented by introducing the initial velocity in solving the nonlinear dynamic analysis algorithm. From the conservation of momentum law, the initial velocity of the structure v_2 is calculated by $v_2 = m_1 v_1/(m_1 + m_2)$, where m_1 and v_1 represent the mass and the velocity of the dropping mass, and m_2 is the total mass of beam. In advance, the velocity v_1 is determined on the basis of the energy conservation law and has a value of $v_1 = 8.0$ m/s. For the idealization of this beam, ten elements including two smaller elements at the mid-span whose length is $l = 360$ mm, which is less than the plastic hinge length of $l_p = 369$ mm, are used and an additional two elements with $l = 940$ mm are considered to idealize the overhang part. Upon the determination of the initial velocity of beam and the defined impact loading history in Fig. 12, a nonlinear dynamic time history analysis was conducted.

As shown in Fig. 13, the numerical results obtained by considering the bond-slip effect and the loading history of the constituent materials show a good correlation with experimental data and lead to accurate predictions compared with those obtained when ignoring both effects. Moreover, the comparison of the displacement history after the post-peak response shows the importance of considering both effects. These effects appear to be more remarkable in the case of RC beams accompanying large displacements by the yielding of reinforcing steel (see Fig. 13). However, Fig. 13b shows that the obtained numerical results represent a slight difference from the experimental data in the displacement history. This difference seems to be caused by the linear simplification of the impact loading history after 2 ms (see the dashed line in Fig. 12b). Since the large deformation usually leaves residual deformation in a structural member while preventing the structure from returning to its original position, an inaccurate prediction of the displacement history in a structural member may cause a wrong evaluation of the ultimate resisting capacity of the entire structure damaged by the blast and impact loadings.

Besides, differently from experimental data in the beam SS3b, which represents a rapid decrease of the returning period from the second half of the first fluctuation in the displacement history, the numerical model still sustains almost the same returning period regardless of the number of displacement cycles (see Fig. 13b). This means that the beam model may have a limitation in simulating the local effect induced by repetition of the crack opening and closing after experiencing the large deformation because the formulation of the beam element is basically based on the continuum displacement field, which does not allow discontinuity in the deformation.

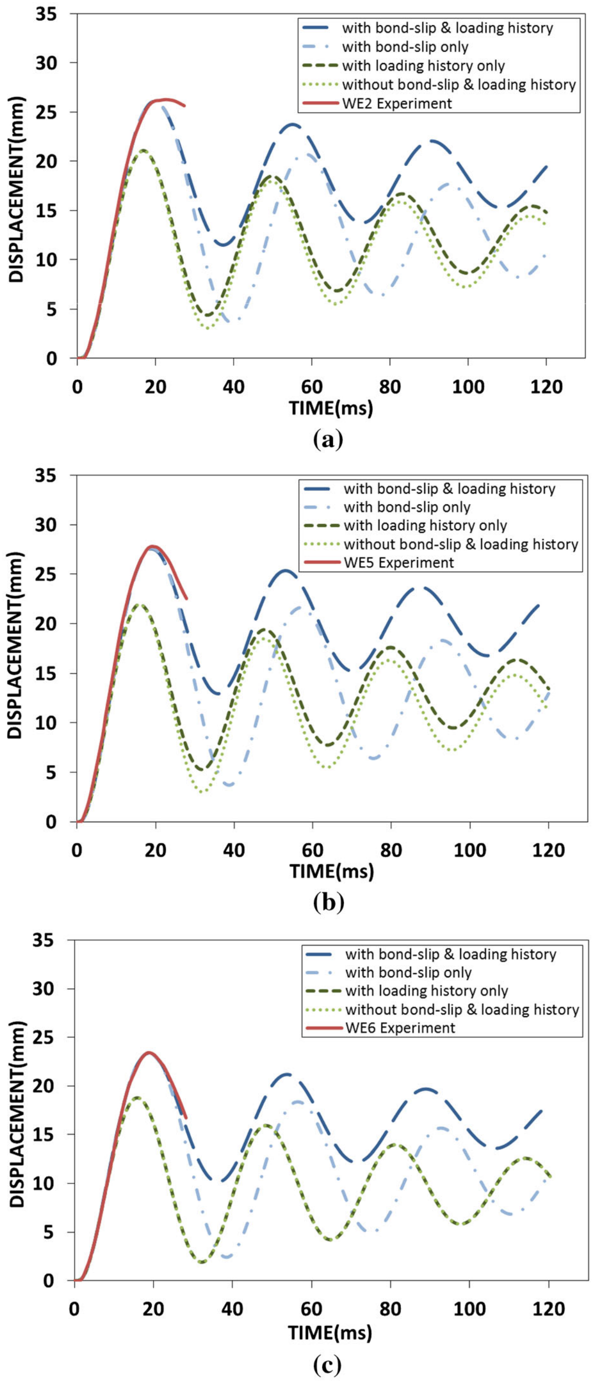

Fig. 10 Mid-span deflection with time for WE beams. **a** WE2, **b** WE5, and **c** WE6.

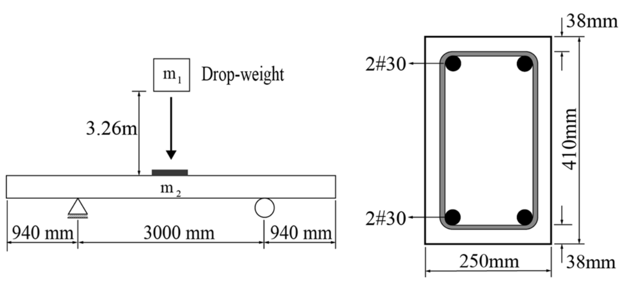

Fig. 11 Geometry of beams SS3a and SS3b (Saatci 2007).

On the other hand, as shown in Fig. 14, the numerical results obtained by considering only one effect represent larger differences from the experimental data. In particular, Fig. 14 represents the relative importance of considering the loading history of the constituent materials in these RC beams. After reaching the maximum deflection at the mid-span at the first loading phase, which was developed by the yielding of steel (phase a, b in Fig. 14b), the structural response accompanies the unloading behavior with a decrease in the developed deflection (phase b, c in Fig. 14b). In this stage, the absence of consideration of the loading history of steel forces the unloading phase of steel to follow the monotonic envelope curve, which has very small stiffness at the yielding stage. Accordingly, because of the very small stiffness of steel, no consideration of the loading history shows a larger variation in the mid-span deflections, as shown in Fig. 14. The same explanation can also be considered for the WE series specimens subjected to blast loadings, and the reason for an increase of the return period will be the same as that described in the previous example.

The beam SS3a was also analyzed by the SDOF method, and Fig. 15 compares the displacement histories obtained by the introduced numerical model and the SDOF method with the experimental results. The SDOF method gives very satisfactory predictions of the displacement history. As mentioned before, the SDOF method can effectively be used when the structural response is relatively small before yielding of reinforcing steel. However, as shown in Fig. 15b, the most reasonable result was obtained when the damping ratio was assumed as 9% of the critical damping ratio, but this ratio is quite different from the usually used damping ratio of 3–4% of the critical damping ratio in RC structures. Moreover, an increase of the damping ratio causes a decrease of the maximum displacement. This means that the use of the SDOF method to trace the displacement history after reaching the maximum displacement may have some limitations because the application procedure of the SDOF method not only contains a lot of approximation, which makes it difficult to obtain reliable results, as was mentioned by many researchers (Carta and Stochino 2013; Guner 2016), but also has a limitation in application to multi-degree of freedom structures composed of many structural members.

6. Conclusion

This paper introduces an improved layered section model that can simulate the nonlinear dynamic analysis of RC beams subjected to blast and impact loadings. Unlike the classical layered section approach that usually gives conservative structural responses because of the absence of consideration of the bond-slip effect, the introduced numerical model takes into account the bond-slip between reinforcing steel and surrounding concrete by changing the bending stiffness EI of elements placed within the plastic hinge length, and the consideration of the bond-slip effect leads to a remarkable improvement in the accuracy of the

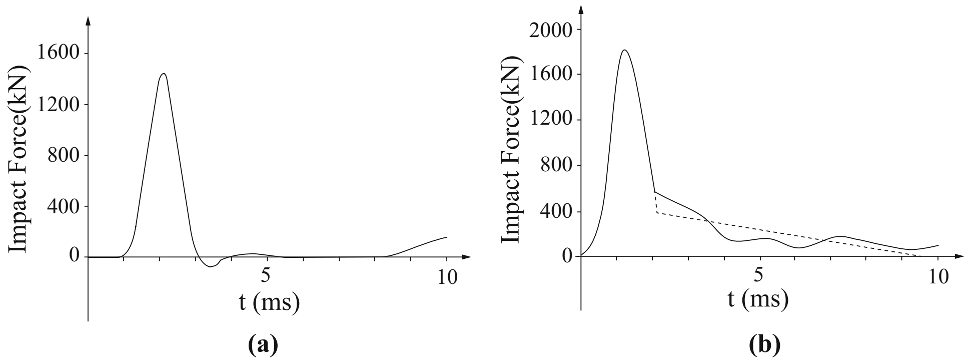

Fig. 12 Impact force–time history for beams **a** SS3a and **b** SS3b.

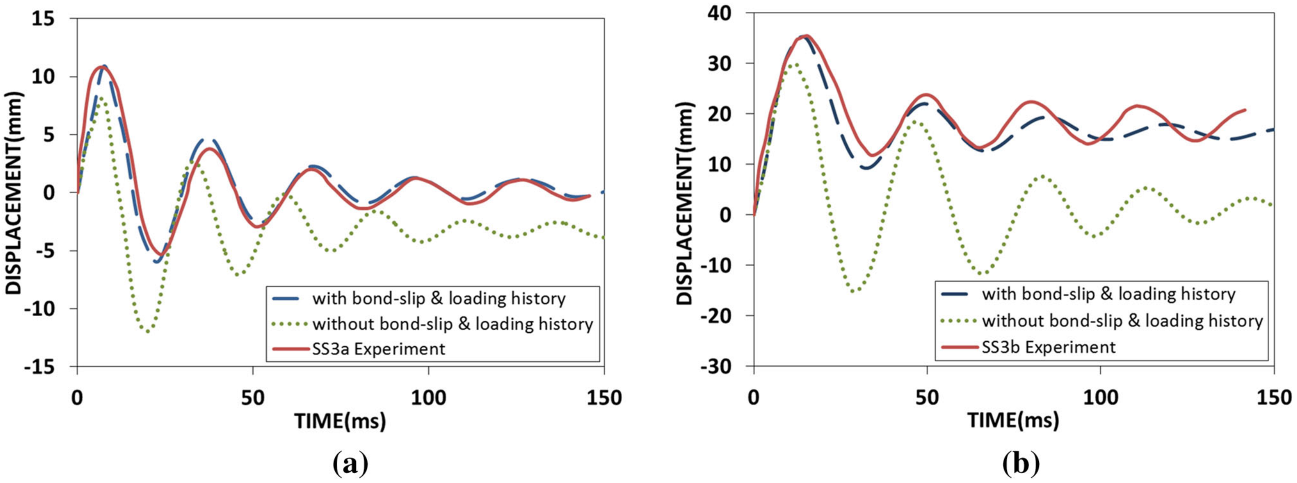

Fig. 13 Comparison of mid-span deflection with time for beams **a** SS3a and **b** SS3b.

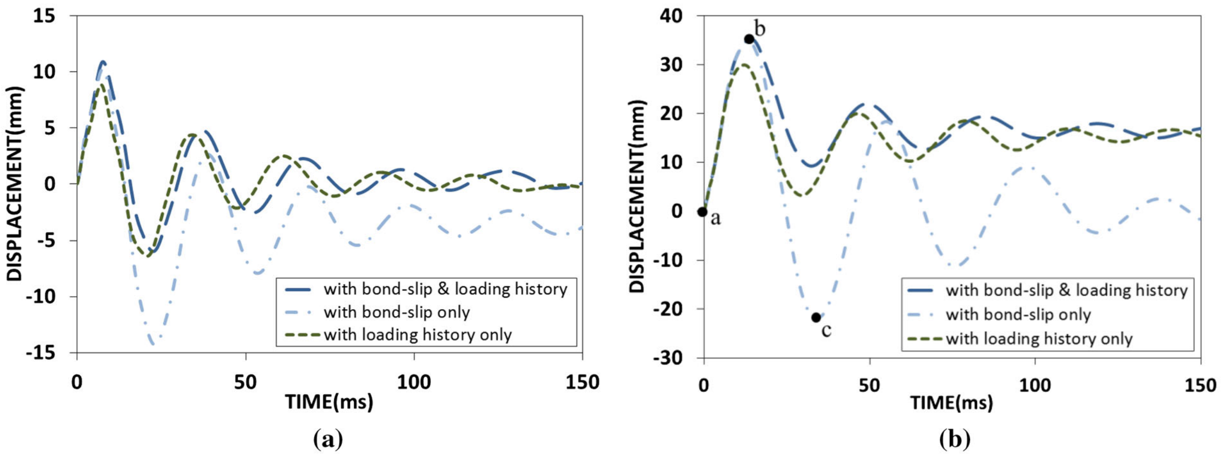

Fig. 14 Mid-span deflection with time for beams **a** SS3a and **b** SS3b, considering bond-slip and loading history.

numerical results. Moreover, the consideration of the loading history in the constituent materials makes it possible to trace the structural response after reaching the maximum response. Through correlation studies between the numerical results and experimental data, the following conclusions are reached: (1) to improve the accuracy of the simulation results in RC beams, the bond-slip effect and the loading history of the constituent materials must be considered. In particular, the importance of considering the bond-slip effect needs to be emphasized; (2) the SDOF method has a limitation in application to RC beams with large deformation induced by the yielding of reinforcing steel; and (3) the proposed model can be used effectively in predicting the structural response of entire RC structures subjected to blast and impact loadings; nevertheless, (4) it is also true that the proposed model has a limitation in simulating the shear-dominant structural behavior.

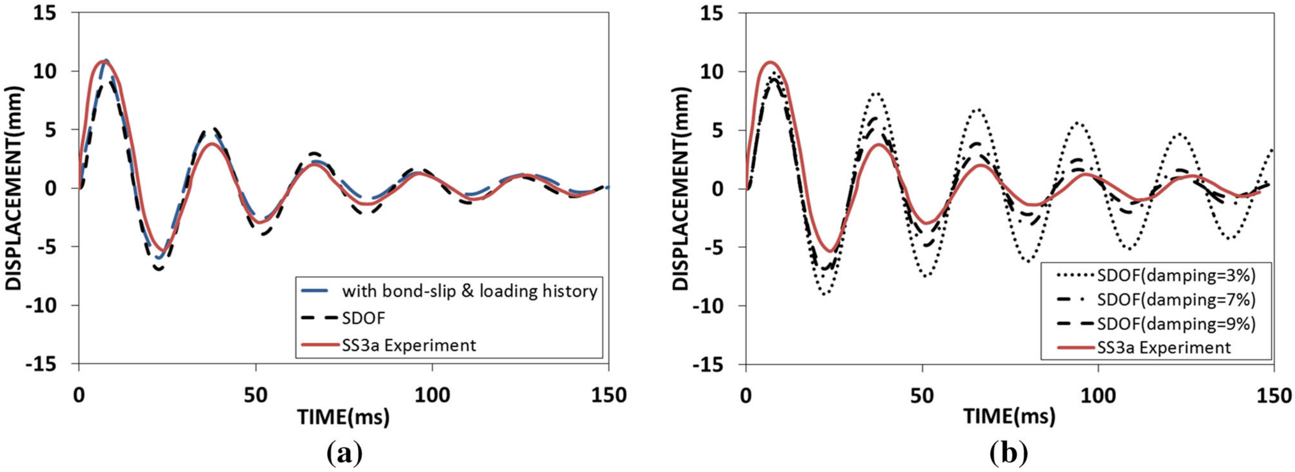

Fig. 15 Mid-span deflection time history including SDOF for SS3a.

Acknowledgements

This work was supported by the National Research Foundation of Korea (NRF) Grant funded by the Korean Government (MSIP) (No. 2017R1A5A1014883), and this research was supported by a Construction Technology Research Project (17SCIP-B128706-01) funded by the Ministry of Land, Infrastructure and Transport.

Open Access

References

ACI Committee, & ACI. (2008). Building code requirements for structural concrete (ACI 318-08) and commentary.

Ayoub, A., & Filippou, F. C. (1999). Mixed formulation of bond-slip problems under cyclic loads. *Journal of Structural Engineering, 125*(6), 661–671.

Bayrak, O., & Sheikkh, S. (1997). High-strength concrete columns under simulated earthquake loading. *ACI Structural Journal, 94*(6), 708–722.

Belarbi, A., & Hsu, T. T. C. (1994). Constitutive laws of concrete in tension and reinforcing bars stiffened by concrete. *ACI Structural Journal, 91*(4), 465–474.

Bicanic, N., de Borst, R., Mang, H., & Meschke, G. (2011). *Computational modelling of concrete structures*. Boca Raton: CRC Press.

Biggs, J. M. (1964). *Introduction to structural dynamics*. New York: McGraw-Hill.

Cadoni, E., Solomos, G., & Albertini, C. (2009). Mechanical characterisation of concrete in tension and compression at high strain rate using a modified Hopkinson bar. *Magazine of Concrete Research, 61*(3), 221–230.

Carta, G., & Stochino, F. (2013). Theoretical models to predict the flexural failure of reinforced concrete beams under blast loads. *Engineering Structures, 49,* 306–315.

Chen, G. M., Chen, J. F., & Teng, J. G. (2012). On the finite element modelling of RC beams shear-strengthened with FRP. *Construction and Building Materials, 32,* 13–26.

Comite Euro-International. (1993). *Ceb-fip model code 1990: Design code du beton*. Wiltshire: Redwood Books.

Craig, R. R., Jr., & Kurdila, A. J. (2006). *Fundamentals of structural dynamics* (2nd ed.). Hoboken: Wiley.

Cusatis, G. (2011). Strain-rate effects on concrete behavior. *International Journal of Impact Engineering, 38*(4), 162–170.

Filippou, F. C., Popov, E. P., & Bertero, V. V. (1983). *Effects of bond deterioration on hysteretic behaviour of reinforced concrete joints*. Berkeley, CA: Earthquake Engineering Research Center.

Fujikake, K., Li, B., & Soeun, S. (2009). Impact response of reinforced concrete beam and its analytical evaluation. *Journal of Structural Engineering, 135*(8), 938–950.

Fujikura, S., & Bruneau, M. (2011). Dynamic analysis of multihazard-resistant bridge piers having concrete-filled steel tube under blast loading. *Journal of Bridge Engineering, 17*(2), 249–258.

Gergely, P., & Lutz, L. A. (1968). Maximum crack width in reinforced concrete flexural members, *Sp 20-6*, 87–117.

Guner, S. (2016). Simplified modeling of frame elements subjected to blast loads. *ACI Structural Journal, 113*(2), 363–372.

Hao, Y., Hao, H., & Zhang, X. H. (2012). Numerical analysis of concrete material properties at high strain rate under direct tension. *International Journal of Impact Engineering, 39*(1), 51–62.

Hibbitt, & Karlsson and Sorenson Inc. (2001). *ABAQUS/standard user's manual*. Providence, RI: Hibbitt, & Karlsson and Sorenson Inc.

Jones, J., Wu, C., Oehlers, D. J., Whittaker, A. S., Sun, W., Marks, S., et al. (2009). Finite difference analysis of simply supported RC slabs for blast loadings. *Engineering Structures, 31*(12), 2825–2832.

Karsan, I. D., & Jirsa, J. O. (1969). Behavior of concrete under compressive loadings. *Journal of the Structural Division, 95*(12), 2543–2563.

Kent, D. C., & Park, R. (1971). Flexural members with confined concrete. In *Journal of the Structural Division* (Vol. 97(ST7), pp. 1969–1990). Reston: American Society of Civil Engineers.

Konstantinidis, D. K., Kappos, A. J., & Izzuddin, B. A. (2007). Analytical stress-strain model for high-strength concrete members under cyclic loading. *Journal of Structural Engineering, 133*(4), 484–494.

Kwak, H. G., & Gang, H. G. (2015). An improved criterion to minimize FE mesh-dependency in concrete structures under high strain rate conditions. *International Journal of Impact Engineering, 86,* 84–95.

Kwak, H. G., & Hwang, J. W. (2010). FE model to simulate bond-slip behavior in composite concrete beam bridges. *Computers & Structures, 88*(17), 973–984.

Kwak, H. G., & Kim, J. K. (2006). Implementation of bond-slip effect in analyses of RC frames under cyclic loads using layered section method. *Engineering Structures, 28*(12), 1715–1727.

Kwak, H. G., & Kim, S. P. (2010). Simplified monotonic moment-curvature relation considering fixed-end rotation and axial force effect. *Engineering Structures, 32*(1), 69–79.

Lin, X., Zhang, Y. X., & Hazell, P. J. (2014). Modelling the response of reinforced concrete panels under blast loading. *Materials and Design, 56,* 620–628.

Livermore Software Technology Corporation (LSTC). (2007). *LS-DYNA Keyword User's Manual Version 97*, Livermore, CA.

Lowes, L. N., Moehle, J. P., & Govindjee, S. (2004). Concrete-steel bond model for use in finite element modeling of reinforced concrete structures. *ACI Structural Journal, 101,* 501–511.

Luccioni, B., Ambrosini, R., & Danesi, R. (2004). Analysis of building collapse under blast loads. *Engineering Structures, 26*(1), 63–71.

Magnusson, J. (2007). Structural concrete elements subjected to air blast loading, Dissertation.

Magnusson, J., & Hallgren, M. (2000). *High performance concrete beams subjected to shock waves from air blast*. Tumba, Sweden.

Mashaly, E.-S., El-Heweity, M., Abou-Elfath, H., & Ramadan, M. (2011). A new beam-column model for seismic analysis of RC frames—Part I: Model derivation. *Alexandria Engineering Journal, 50*(4), 313–320.

Menegotto, M., & Pinto, P. E. (1973). Method of analysis for cyclically loaded R.C. plane frames including changes in geometry and non-elastic behaviour of elements under combined normal force and bending. In *IABSE reports of the working commissions* (Vol. 13).

Monti, G., & Spacone, E. (2000). Reinforced concrete fiber beam element with bond-slip. *Journal of Structural Engineering, 126,* 654–661.

Oliveira, R. S., Ramalho, M. A., & Corrêa, M. R. S. (2008). A layered finite element for reinforced concrete beams with bond-slip effects. *Cement & Concrete Composites, 30*(3), 245–252.

Ožbolt, J., & Sharma, A. (2011). Numerical simulation of reinforced concrete beams with different shear reinforcements under dynamic impact loads. *International Journal of Impact Engineering, 38*(12), 940–950.

Qu, Y., Li, X., Kong, X., Zhang, W., & Wang, X. (2016). Numerical simulation on dynamic behavior of reinforced concrete beam with initial cracks subjected to air blast loading. *Engineering Structures, 128,* 96–110.

Saatci, S. (2007). *Behaviour and modelling of reinforced concrete structures subjected to Impact Loads.* Ph.D. Thesis. University of Toronto, Toronto.

Saatcioglu, M., Lloyd, A., Jacques, E., Braimah, A., & Doudak, G. (2011). *Focused research for development of a CSA standard on design and assessment of buildings subjected to blast loads*. Ottawa: University of Ottawa.

Santos, J., & Henriques, A. A. (2015). New finite element to model bond–slip with steel strain effect for the analysis of reinforced concrete structures. *Engineering Structures, 86,* 72–83.

Scott, B. D., Park, R., & Priestley, M. J. N. (1982). Stress–strain behavior of concrete confined by overlapping hoops at low and high strain rates. *Journal Proceedings, 79*(1), 13–27.

Seabold, R. H. (1967). *Dynamic shear strength of reinforced concrete beams, part 2*. Port Hueneme, CA: US Naval Civil Engineering Laboratory.

Shkolnik, I. E. (2008). Influence of high strain rates on stress-strain relationship, strength and elastic modulus of concrete. *Cement & Concrete Composites, 30*(10), 1000–1012.

Tachibana, S., Masuya, H., & Nakamura, S. (2010). Performance based design of reinforced concrete beams under impact. *Natural Hazards and Earth System Science, 10*(6), 1069–1078.

Taucer, F. F., Spacone, E., & Filippou, F. C. (1991). *A fiber beam-column element for seismic response analysis of reinforced concrete structures*. Report No. UCB/EERC-91/17. Berkeley, CA.

Tu, Z., & Lu, Y. (2009). Evaluation of typical concrete material models used in hydrocodes for high dynamic response simulations. *International Journal of Impact Engineering, 36*(1), 132–146.

US DoD. (2008). *Unified facilities criteria (Ufc) structures to resist the effects of accidental*. Washington, DC: Department of Defence.

Valipour, H. R., Huynh, L., & Foster, S. J. (2009). Analysis of RC beams subjected to shock loading using a modified fibre element formulation. *Computers and Concrete, 6*(5), 377–390.

Wu, Y., Crawford, J. E., & Magallanes, J. M. (2012). Performance of LS-DYNA concrete constitutive models. In *12th International LS-DYNA Users conference* (pp. 1–14).

Yan, D., & Lin, G. (2006). Dynamic properties of concrete in direct tension. *Cement and Concrete Research, 36*(7), 1371–1378.

Yao, S. J., Zhang, D., Lu, F. Y., Wang, W., & Chen, X. G. (2016). Damage features and dynamic response of RC beams under blast. *Engineering Failure Analysis, 62,* 103–111.